ELSEVIER

Solid State Ionics 94 (1997) 99–114

SOLID STATE IONICS

Reconstruction phenomena at gold/electrolyte interfaces: an in-situ STM study of Au(100)

A.S. Dakkouri[1]

Department of Electrochemistry, University of Ulm, D-89069 Ulm, Germany

Abstract

The structure of Au(100) surfaces in contact with aqueous solutions has been studied by in-situ scanning tunnelling microscopy. It is shown that the surface topography of flame annealed Au(100) sensitively depends on the sample preparation as well as on the electrochemical pretreatment. Flame annealed Au(100) surfaces are reconstructed and it is demonstrated under which conditions this initial (thermally induced) reconstruction is preserved during and after contact with the electrolyte. Once the initial reconstruction of a gold surface has disappeared, e.g. due to specific adsorption of anions, a potential induced reconstruction may take place, usually at potentials clearly negative with respect to the potential of zero charge. As a consequence, the surface structure of an Au(100) electrode is potential dependent and structural changes may occur within the potential region chosen for an electrochemical experiment. The kinetics and a mechanistic model of the structural transition are briefly discussed.

Keywords: Surface reconstruction; Gold single crystal surfaces; Au(100); Scanning tunnelling microscopy (STM)

1. Introduction

The surface structure of metal electrodes plays a decisive role in many electrochemical reactions, particularly in electrocatalysis. For an atomistic view of electrode processes, however, it is almost mandatory to use single crystals with structurally well-defined surfaces, because surfaces of polycrystalline materials are far too complex to allow a mechanistic interpretation. Only from measurements with single crystal electrodes did we learn about the pronounced structure sensitivity of many electrochemical reactions such as the oxidation of organic fuel [1], the reduction of oxygen [2] and the formation of thin metallic overlayers [3]. With the use of single crystal material it is assumed tacitly that the atoms at the surface retain their bulk positions and hence, the surface structure can be derived directly from the bulk structure. Although many metal surfaces fulfil this expectation, some do not. The reason for this deviation is the break in translational symmetry at a surface. Therefore, atoms at surfaces experience different forces than atoms in the bulk, which very often leads to a rearrangement in the top layer with respect to the bulk structure: (i) quite often, small variations in the bond length normal to the surface are found for atoms in the surface region in response to the changed environment. Typically, there is a contraction of the spacing between the first and second atomic layers (of the order of a few percent

[1] Present address: Lehrstuhl für Korrosion und Oberflächentechnik, Friedrich-Alexander-Universität Erlangen-Nürnberg, Martensstr. 7, D-91058 Erlangen (Germany)

PII S0167-2738(96)00499-7

of the bulk spacing), followed by an expansion between the next two layers. This effect is called surface relaxation. (ii) Within the surface there may also be local bond breaking and new bond formation which we call surface reconstruction. In this case, surface atoms undergo a lateral displacement which is driven by a lowering of the surface energy and is often connected with phase transitions to markedly different surface structures. (iii) It is also possible that a clean surface can undergo larger-scale changes facilitated by surface diffusion over distances that are much greater than atomic spacings. Such a surface restructuring – which is called surface reshaping – can cause macroscopic changes in the surface topography, e.g. creation of steps, surface roughening and faceting.

It is well established from ultrahigh vacuum (UHV) studies that all three low index faces of a gold single crystal reconstruct when they are subjected to a heat treatment [4–6]. For example, the Au(100) surface reconstructs into a hexagonal close packed (hcp) form (see Fig. 1(a)) [7,8] which will be called in the following '(hex)'-structure. The (110) surface of gold typically reconstructs into the (1×2)-'missing row', in which every second row of atoms has been removed to yield narrow (111)-microfacets in the [110] direction [6,9,10] (Fig. 1(b)). Occasionally, a (1×3) or $(1 \times n)$ (with $n = 5, 7,...$) reconstruction is observed with correspondingly deeper grooves and larger (111)-microfacets. Although already densely packed, Au(111) shows a so-called $(\sqrt{3} \times 22)$ reconstruction which consists of a slight lateral compression of the surface atoms in one of the three [110] directions by about 4.4%. This causes every 23rd surface atom to be in register with the underlying bulk. Correspondingly, the unit cell of this reconstruction, about 6.3 nm, is rather large (see Fig. 1(c)).

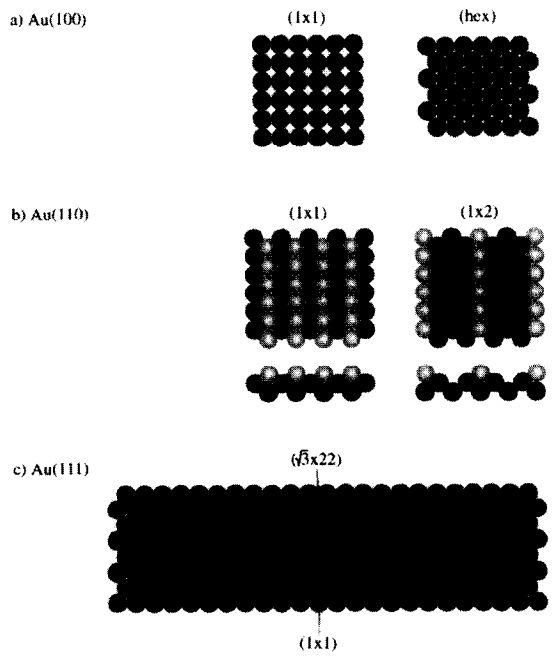

Fig. 1. The structure of unreconstructed and reconstructed gold single crystal surfaces.

Although a clean, reconstructed surface may be thermodynamically more stable than the unreconstructed one, there is an activation barrier that prevents spontaneous reconstruction at room temperature. This activation barrier can be substantial in height, because in most cases reconstruction involves bond breaking and a transport of atoms rather than a simple displacement of surface atoms within their unit cell. Therefore, in UHV the unreconstructed surface is generally trapped in its metastable state and additional energy has to be applied, e.g. by a heat treatment, in order to restore the reconstructed surface.

In the following, the role of surface reconstruction in electrochemistry will be demonstrated for Au(100), where surface reconstruction has the largest impact on the physical and electrochemical properties of the surface of all three low-index faces of gold.

2. Electrochemical scanning tunnelling microscopy

Although surface reconstruction of electrodes had been studied before by a number of different techniques, the scanning tunnelling microscope (STM) has contributed in a very important way to a detailed (atomistic) understanding of those phenomena. This technique offers not only the fascinating possibility to image surfaces with atomic resolution but also allows the direct, real space determination of surface structures in three dimensions, including non-periodic (defect) structures. In Fig. 2(a) the principle of

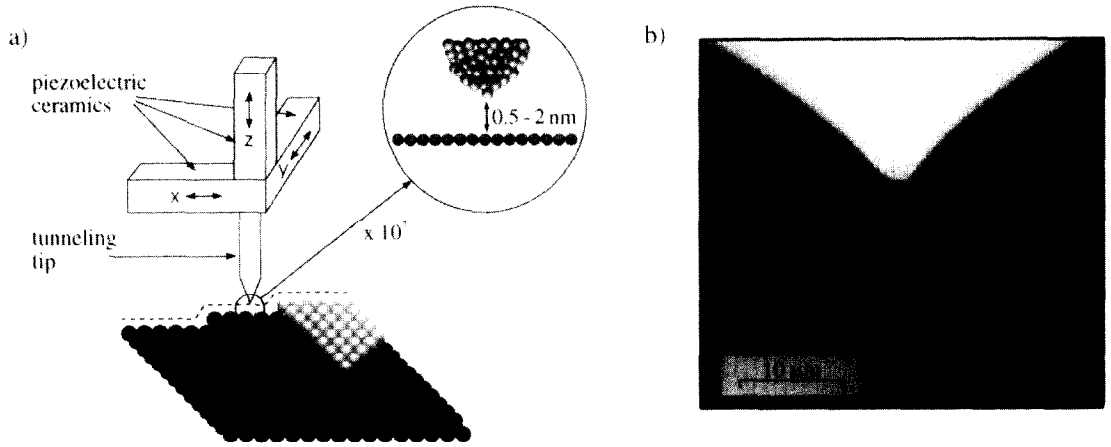

Fig. 2. (a) Schematic diagram, showing the principle of STM; (b) scanning electron micrograph of a tungsten tip which has been coated with Apiezon® wax. The tip radius is less than 70 nm.

STM is described: A fine metal tip which acts as a local probe is brought into close proximity with the (conductive) surface under study. By applying a voltage between tip and sample, the so-called tunnelling voltage V_t, electrons will tunnel from one side to the other, giving rise to a tunnelling current I_t. An image of the surface is obtained by scanning the tip line by line across the surface. This scanning process is controlled by a system of piezoelectric ceramics which allows both vertical and horizontal movements of the tip in the range of Angstroms. Simultaneously, an electronic feedback circuit controls the vertical position of the tip in such a way that the tunnelling current is maintained at a constant value ('constant current mode'). Consequently, the z-position of the tip changes as it scans for example across an atomic step and, hence, the surface topography is directly reflected by the z-piezo voltage as a function of the x,y-position of the tip. With STM a resolution of about 0.1 nm laterally and 0.01 nm vertically can be achieved. This extraordinary high vertical resolution is caused by an exponential dependence of the tunnelling current I_t on the tip-to-sample spacing s:

$$I_t \propto V_t \exp\left[- A \sqrt{\langle \Phi_t \rangle}\, s \right]$$

with $A = 10.25\ \mathrm{nm}^{-1}\ (\mathrm{eV})^{-1/2}$ and $\langle \Phi_t \rangle$ = mean barrier height. That means, varying the tunnelling distance by only the diameter of one atom changes the tunnelling current by about three orders of magnitude.

In an electrochemical STM, the metal tip is immersed in the electrolyte and hence inevitably acts as a fourth electrode. In general, there will be an electrochemical current flowing at the tip/electrolyte interface which is superimposed onto the tunnelling current and which cannot be distinguished from the latter by the feedback control. Therefore, a large portion of the tip is isolated by appropriate means (e.g. glass [11], wax [12] or polymer coating [13]) to reduce the area which is in contact with the electrolyte. The scanning electron micrograph in Fig. 2(b) shows a tungsten tip coated with Apiezon® (a thermoplastic wax). This procedure leaves typically less than 10 μm of the tip accessible to the electrolyte, which results in an electrochemically active area of about 10^{-7}–10^{-8} cm^2. Additionally, the potential of the tip is controlled independently of that of the sample under study and is generally held in a region where charge transfer reactions are minimal. With these two precautions the electrochemical current is usually less than 50 pA, as compared to the tunnelling currents of typically 1–10 nA. A wide variety of tip material has been used for in-situ STM measurements including W, Ta, Au, Pt and Pt/Ir alloys. All STM experiments shown in the following have been conducted with W-tips, which are prepared by electrochemical etching in an electrolyte lamelle as described in the literature [14].

In the following, STM images are represented as topviews with darker colours corresponding to lower surface areas and lighter colours to higher surface areas, respectively. To record one STM image took usually 1 to 2 min. Hence, with STM it is also possible to follow dynamic processes on the surface in real time, which provides new information about the mechanism and the kinetics of structural transitions between reconstructed and unreconstructed surfaces.

3. Reconstruction of Au(100)

The Au(100) surface is a favourite subject in studies of reconstruction phenomena because in this case there are considerable differences in the structure and density of the topmost layer for the reconstructed and unreconstructed phase. The hexagonal close packed form of reconstructed Au(100), (hex)-form (Fig. 3(a)), contains about 24% more surface atoms than the unreconstructed square lattice (Fig. 3(b)). This unreconstructed Au(100)-(1×1) surface undergoes a structural rearrangement into the (hex)-form when it is subjected to a heat treatment, e.g. by the so-called flame annealing which provides the necessary surface mobility. On the other hand reconstruction is generally removed (lifted) by adsorption of atoms or molecules. This is normally understood in terms of an adsorption that is energetically more favourable on the structurally more open (1×1)-surface than on the densely-packed reconstructed phase. An example for such an adsorbate-induced lifting of reconstruction is CO on Pt(100): When CO is adsorbed on the surface, the (1×1)-structure is the thermodynamically more stable one [15,16]. This implies that the difference in the heats of adsorption for reconstructed and unreconstructed surfaces is large enough to overcompensate the gain in surface energy due to reconstruction; the surface reverts to the unreconstructed case.

The significant structural misfit between the hexagonal close packed top layer and the underlying (100) bulk causes the surface to become slightly buckled and, hence, the reconstructed Au(100) differs somewhat in its properties from a genuine (111) surface. As clearly seen in Fig. 3(c), there is a one-directional long-range corrugation of 1.45 nm periodicity and ca. 0.05 nm height. These so-called reconstruction rows, which are often aligned along terrace steps, are usually taken as indication of a reconstructed surface, because these lines are readily seen even under conditions (i.e. wider scans) where individual surface atoms are no longer visible. This is demonstrated in Fig. 3(e) and Fig. 4.

It is well established that the clean surface of Au(100) is reconstructed when prepared under ultra-high vacuum conditions. But it was not clear at all for a long time whether or not reconstruction phenomena play a role for metal/electrolyte interfaces, because surface reconstruction is usually destroyed by adsorption. The omnipresent water molecules and ions at electrode surfaces could well have rendered reconstruction in an electrochemical environment impossible. At first, the existence of surface reconstruction at the gold/electrolyte interface was postulated by Hamelin [17] in order to explain certain features in cyclic voltammograms of gold single crystal electrodes. But a definite proof had to wait until structure-sensitive techniques became available in electrochemical studies. Yeager and coworkers were the first to show by a combined electrochemical and LEED study that a reconstructed surface (in this case it was reconstructed Pt(110)) is stable even in contact with the electrolyte [18,19]. In the meantime a wide variety of ex-situ and in-situ studies has shown that the (hex)-structure is also stable in contact with an aqueous electrolyte, but only at electrode potentials where the specific adsorption of anions is avoided [20,21]. The latter is usually detrimental to reconstruction.

The reconstruction of Au(100) is lifted by raising the potential beyond a certain critical value where adsorption of anions starts. Fig. 5 shows a cyclic current–potential curve of an Au(100) electrode in 0.1 M H_2SO_4. At negative potentials the reconstructed (hex)-phase is stable. By changing the potential in anodic, i.e. positive, direction, the surface structure changes suddenly to (1×1) which is seen as a pronounced current maximum at +0.37 V vs. SCE. The STM image in Fig. 3(d) shows such an unreconstructed Au(100) surface, where the square lattice arrangement of the individual surface atoms with a next-neighbour distance of 0.29 nm as in the

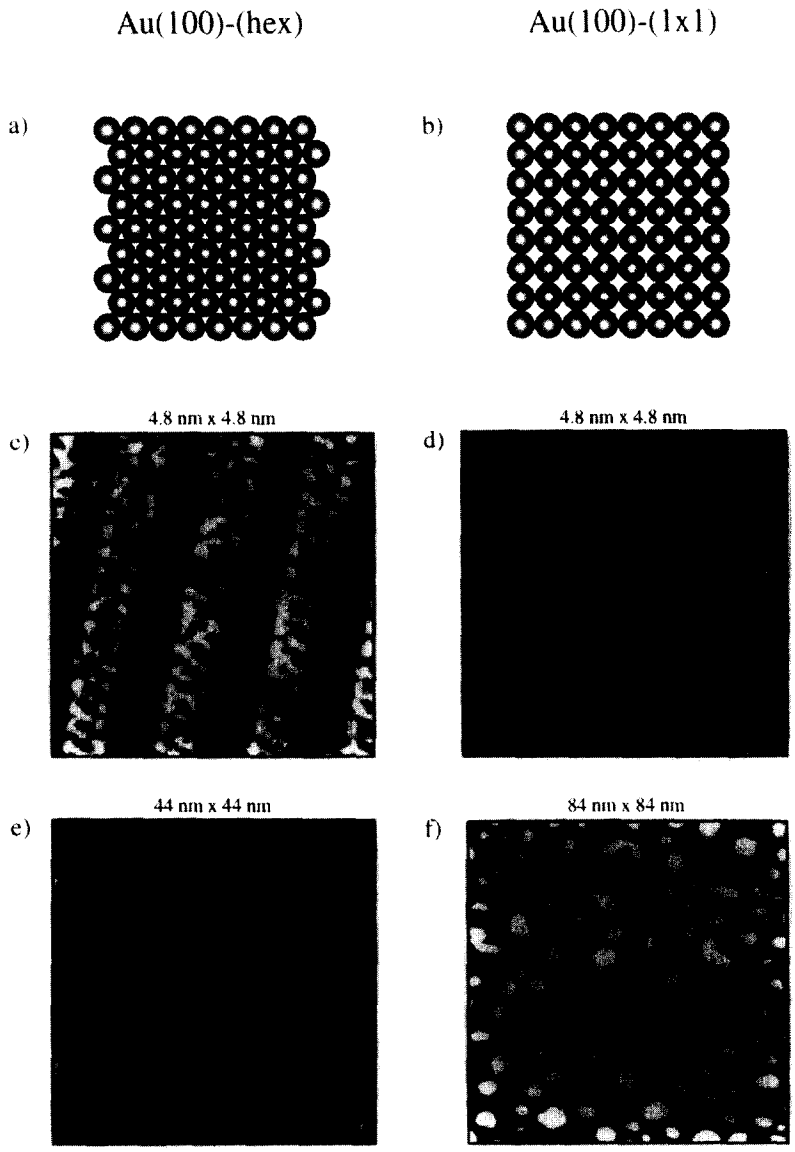

Fig. 3. Models and STM images in 0.1 M H_2SO_4 of the reconstructed (a, c, e) and the unreconstructed (b, d, f) Au(100) surface. $E = -0.24$ V (c), -0.20 V (e), $+0.56$ V (d) and $+0.52$ V (f) vs. SCE. Images (c) and (d) show atomic resolution of a reconstructed and unreconstructed Au(100) surface, while (e) and (f) represent wider scans, emphasizing reconstruction rows and monoatomic-high gold islands, respectively.

bulk is clearly visible. Lifting of reconstruction has another interesting consequence for the surface topography which is demonstrated in Fig. 3(f), a wide-scan STM image of an Au(100) electrode recorded immediately after the (hex)→(1×1) structural transition. Since the reconstructed Au(100) surface has a 24% higher packing density than the unreconstructed one, the excess of gold atoms in the top layer is expelled onto the surface during the transition where monoatomic-high gold islands are formed [22].

The rims of these gold islands, which are inherent

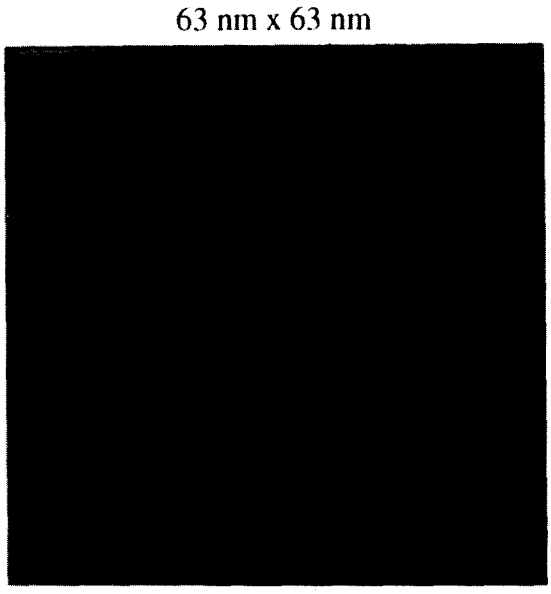

Fig. 4. STM image of a freshly prepared Au(100) electrode in 0.1 M H_2SO_4, showing the initial (thermally induced) reconstruction. $E = -0.24$ V vs. SCE.

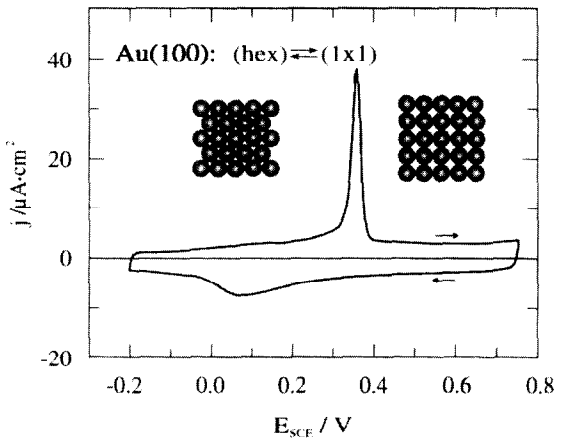

Fig. 5. Cyclic current–potential curve for Au(100) in 0.1 M H_2SO_4, starting with a freshly prepared reconstructed surface at $E = -0.20$ V vs. SCE. Scan rate: 50 mV/s. Lifting of the (hex) reconstruction during the positive scan is seen by a pronounced current peak. The subsequent scan in negative direction reflects the electrochemical behaviour of Au(100)-(1×1).

to unreconstructed gold surfaces after lifting of reconstruction, represent surface defects of considerable density. They can have an impact on the kinetics of surface structural transitions as will be shown later.

4. Preparation of a reconstructed Au(100) surface

As already mentioned, surfaces have to be clean in order to reconstruct and the sample has to be heated to overcome the activation barrier for reconstruction. The classic way of preparing reconstructed surfaces is sputtering and annealing the single crystal in an ultrahigh vacuum chamber. In recent years, the so-called flame annealing was used as a substitute for this rather elaborate and expensive route to well-defined surfaces. This flame annealing was performed first by Clavilier and coworkers [23] by heating a Pt single crystal in a simple Bunsen burner. This method was later adopted for the preparation of single crystal gold electrodes by Hamelin and Katayama [24].

Although sufficiently long annealing of a gold single crystal in a Bunsen flame yields perfectly reconstructed surfaces, this does not warrant the same structure will still be present after immersion in the electrolyte. It has recently been demonstrated that cooling a sample down to room temperature and then contacting it with the electrolyte is of decisive importance for the quality of the reconstructed surface [25]. In the early days of flame annealing, as a simple but very effective means of preparation of clean and well-ordered single crystal surfaces, fast quenching of the hot crystal in ultrapure water was advocated in order to avoid surface contamination by the laboratory air [23,24]. Such a procedure inevitably causes a heat shock to the crystal which can be detrimental to the reconstructed surface as well as to the single crystallinity of the bulk. To demonstrate the crucial role of temperature, we have applied to a Au(100) crystal three different types of cooling procedures after flame annealing [25]. First, the crystal was allowed to cool in air for several minutes until it had reached about room temperature, before it was immersed into the electrochemical cell under potential control. Second, the gold crystal after flame annealing was allowed to cool in air for about 4 s, until the red heat had disappeared, before it was quenched in ultrapure water. The crystal was then

transferred to the electrochemical cell with a droplet of water adhering to the polished surface to protect it from laboratory air. And third, the gold crystal after flame annealing was immediately quenched in ultrapure water in order to eventually reduce the danger of surface contamination in air as much as possible. In all three cases the gold electrodes were immersed into the electrolyte, which was 0.1 M H_2SO_4, under potential control at around −0.20 V vs. SCE. The various topographies of an Au(100) electrode, treated in such ways, are summarized in Fig. 6. The STM images of Fig. 6(a) and (b) show two different regions of a flame annealed Au(100) electrode in 0.1 M H_2SO_4 at −0.15 V vs. SCE and −0.18 V vs. SCE, respectively, which had been cooled in air for 8 min and immersed into the electrolyte at that potential. The surface is well-ordered and completely reconstructed, as seen by the reconstruction rows which cover the whole surface. These results prove beyond any doubt that the initial (thermally induced) surface reconstruction of flame annealed Au(100) can be preserved during and after contact with an aqueous electrolyte, if the electrode potential is sufficiently negative to prevent specific adsorption of anions. No signs of surface contamination were found in the STM images despite cooling the sample in air, indicating that any contaminants were easily removed in the electrolyte.

Fig. 6(c) shows the STM image of Au(100) which was subjected to the second procedure: The crystal was cooled in air for about 4 s and then quenched in ultrapure water. Such a treatment can be considered to be a compromise between the heat shock and the danger of surface contamination in air. The result is a surface which is almost completely reconstructed, the reconstruction rows still covering about 70–80% of the total surface. On some parts of the surface, however, reconstruction has been lifted upon contact with the electrolyte, as is seen by the dark area to the right in Fig. 6(c) and by the monoatomic-high gold islands. Overall, the surface contains large areas which still show the initial reconstruction and, hence, the second treatment is also well-suited for the study of reconstruction phenomena. Fig. 6(d) shows the very same area as Fig. 6(c), but after reconstruction had been lifted by specific adsorption of sulphate ions during a potential cycle up to +0.25 V vs. SCE. This demonstrates once more the difference in the topography of a freshly reconstructed Au(100) and an unreconstructed Au(100) surface immediately after the (hex)→(1×1) transition. The unreconstructed surface is covered with small monoatomic-high gold islands which were formed out of the surface excess of the more densely-packed (hex)-structure [22]. The islands are roughly 1–2 nm in diameter, but they grow with time due to surface diffusion (two-dimensional Ostwald ripening), as will be briefly demonstrated in Section 5. Note that the gold islands in Fig. 6(c), which were obviously generated during the quenching of a crystal which was still at elevated temperatures, are large compared to the islands generated by the anion-induced (hex)→(1×1) transition at room temperature. This could be explained by the higher temperature at which the Ostwald ripening took place during quenching.

Fig. 6(e) shows the STM image of an Au(100) surface which had been subjected to the third treatment: Rapid quenching after flame annealing. Obviously, such a treatment yields a highly disordered surface which seems to be in a rather unreconstructed state, as far as one can judge from the blurred image. Subsequent application of a positive potential scan to lift eventually existing areas with (hex)-structure did not produce extra gold islands (Fig. 6(f)) (the four gold islands in Fig. 6(f) marked by arrows already existed before the potential step, see Fig. 6(e)), supporting our view that rapid quenching does not yield reconstructed surface areas of any significant extent.

5. Stability of reconstructed Au(100) in an electrochemical environment

As has been shown in Fig. 5, the structural transition, (hex)→(1×1), due to lifting of reconstruction is very clearly seen in the cyclic voltammograms of the Au(100) electrode as a pronounced current peak at the transition potential. This current peak arises from the marked difference in the potentials of zero charge (pzc's) of the (hex)- and (1×1)-structure (+0.30 V and +0.08 V vs. SCE in 0.01 M $HClO_4$, respectively [20]), which requires additional double-layer charging during the (hex)→(1×1) transition and the concomitant shift of

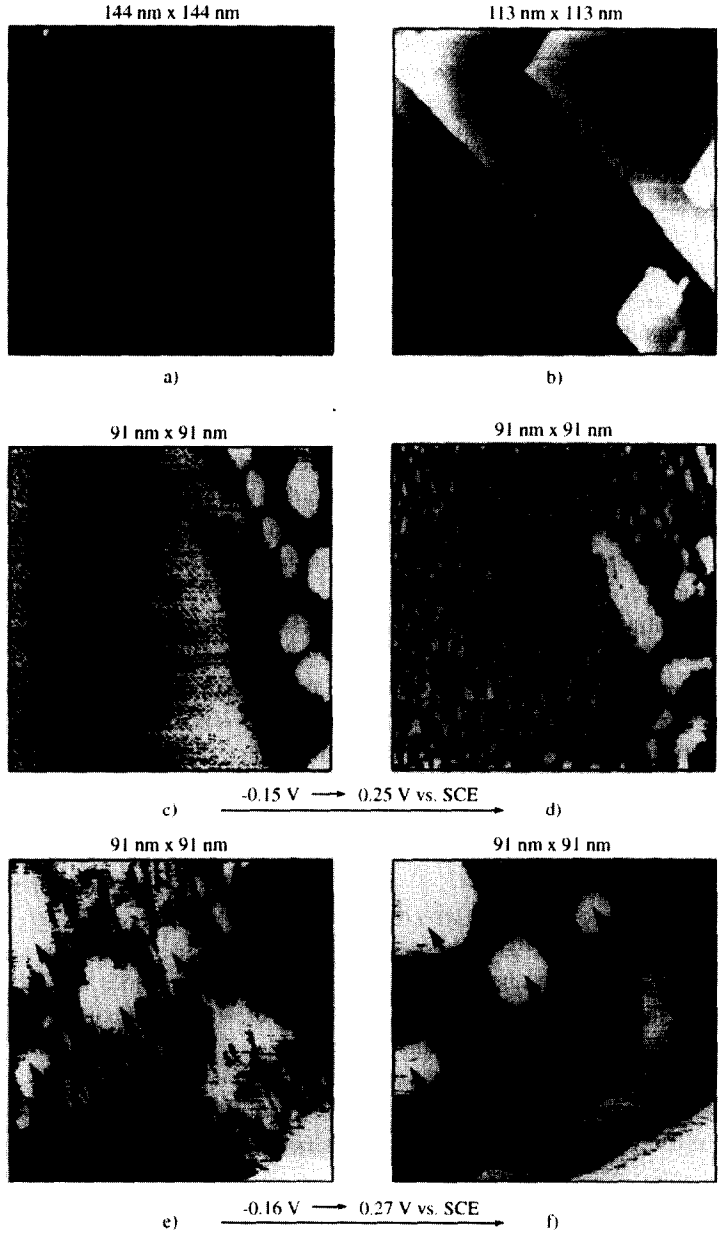

Fig. 6. STM images of flame annealed Au(100) electrodes in 0.1 M H_2SO_4. (a, b) The electrode was cooled in air for 8 min and immersed at $E = -0.15$ V and -0.18 V vs. SCE, respectively. The initial reconstruction is fully preserved. (c) The electrode was cooled in air for 4 s and then quenched in water before immersion into the electrolyte at $E = -0.15$ V vs. SCE. The initial reconstruction is preserved for most parts of the surface. (d) Same area as in (c), but recorded at $E = +0.25$ V vs. SCE, where reconstruction is lifted. (e) The electrode was rapidly quenched in water after flame annealing, before immersion at $E = -0.16$ V vs. SCE. The surface appears highly disordered. (f) Same area as in (e), but recorded at $E = +0.27$ V vs. SCE.

0.22 V in the pzc. In systematic studies, the influence of various organic molecules [26,27] and anions [20] on the transition potential had been determined as a function of their concentrations by cyclic voltammetry. Three such curves showing the current peak due to lifting of the reconstruction in sulphate (solid

curve) and chloride (two concentrations; dashed and dotted curve) are reproduced in Fig. 7. In the presence of the more strongly adsorbing chloride ion, the stability range of the (hex)-structure is clearly reduced. Additionally, the shift of the transition potential in a cathodic direction is more pronounced the higher the concentration of chloride is. A comparison with previously published data [20] and Fig. 5, however, reveals a difference of about 200 mV for the peak potentials, the transition occurring at the more positive values in the present study, where gold crystals with larger terraces were used. A preliminary investigation points towards kinetic reasons as the origin of the discrepancy in peak potentials: Lifting of the reconstruction was shown to follow a nucleation-and-growth process [28], with monoatomic-high steps as the most likely nucleation centres, and the growth of the (1×1)-domains being strictly one-dimensional along the reconstruction rows (see Fig. 8, [22,29]). In the case of large, atomically flat terraces complete removal of the

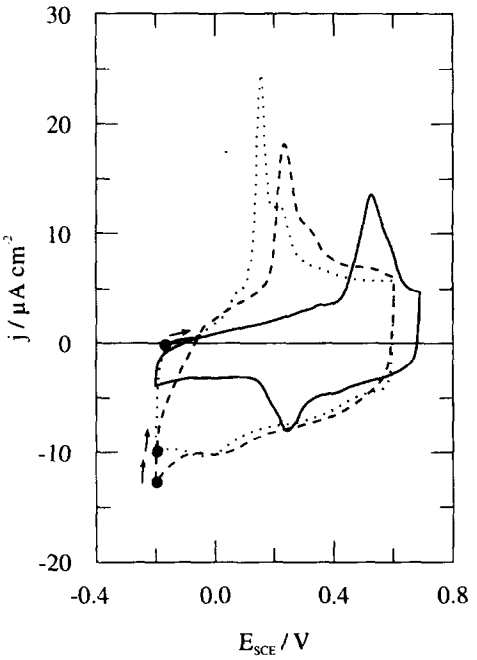

Fig. 7. Cyclic current–potential curves (first scans) for freshly prepared Au(100) electrodes in 0.1 M H_2SO_4 (———), 0.1 mM HCl (- - -) and 1 mM HCl (· · ·). Scan rate: 50 mV/s. Immersion of the freshly prepared Au(100) electrodes at $E = -0.20$ V vs. SCE.

reconstruction takes considerably longer than for less perfectly prepared surfaces with smaller terrace sizes and hence the current peak due to lifting of reconstruction may be shifted to more positive potentials during the anodic scan of a cyclic voltammogram.

5.1. Model for the (hex)→(1×1) transition

The structural changes during lifting of the reconstruction are illustrated in the sequence of STM images in Fig. 8. In the first image the Au(100) surface is reconstructed, the terrace being completely covered with a single (hex)-reconstructed domain. The reconstruction rows are oriented roughly from top to bottom of the image. Only a few missing rows are seen (dark longish areas). Fig. 8(b) shows the same surface area, but at +0.37 V vs. SCE, and it can be seen that unreconstructed areas slowly begin to be formed. Note that at this potential lifting of the reconstruction is not anticipated from the cyclic voltammogram (Fig. 7) which has been recorded on a much shorter time scale. The (1×1)-areas are easily recognized by the formation of monoatomic high gold islands. In Fig. 8(c–e) the lifting of reconstruction occurs at an electrode potential of +0.47 V vs. SCE. It can be clearly seen that this process proceeds by a growth of unreconstructed areas strictly along the direction of the reconstruction rows and no growth of the unreconstructed areas in the perpendicular direction is observed. Finally, after holding the potential at +0.47 V vs. SCE for 18 min, the Au(100) surface is completely unreconstructed, the whole terrace being covered with monoatomic-high gold islands which are also unreconstructed.

In this series of STM images (Fig. 8) it is seen that, due to a slow increase of the electrode potential, the reconstruction is lifted by a growth of unreconstructed areas along the direction of the reconstruction rows. This leads to a quasi one-dimensional growth mechanism for this structure. Although this process is too fast for a direct observation of the atoms' movements by an STM, a possible model is suggested in Fig. 9 which is based on STM results and which shows an atomic level mechanism of the lifting of reconstruction of Au(100) surfaces. The following rearrangement of surface atoms (for easier description some atoms are marked with numbers) takes place: Atoms 1 to 6 and 10 to 13, respectively,

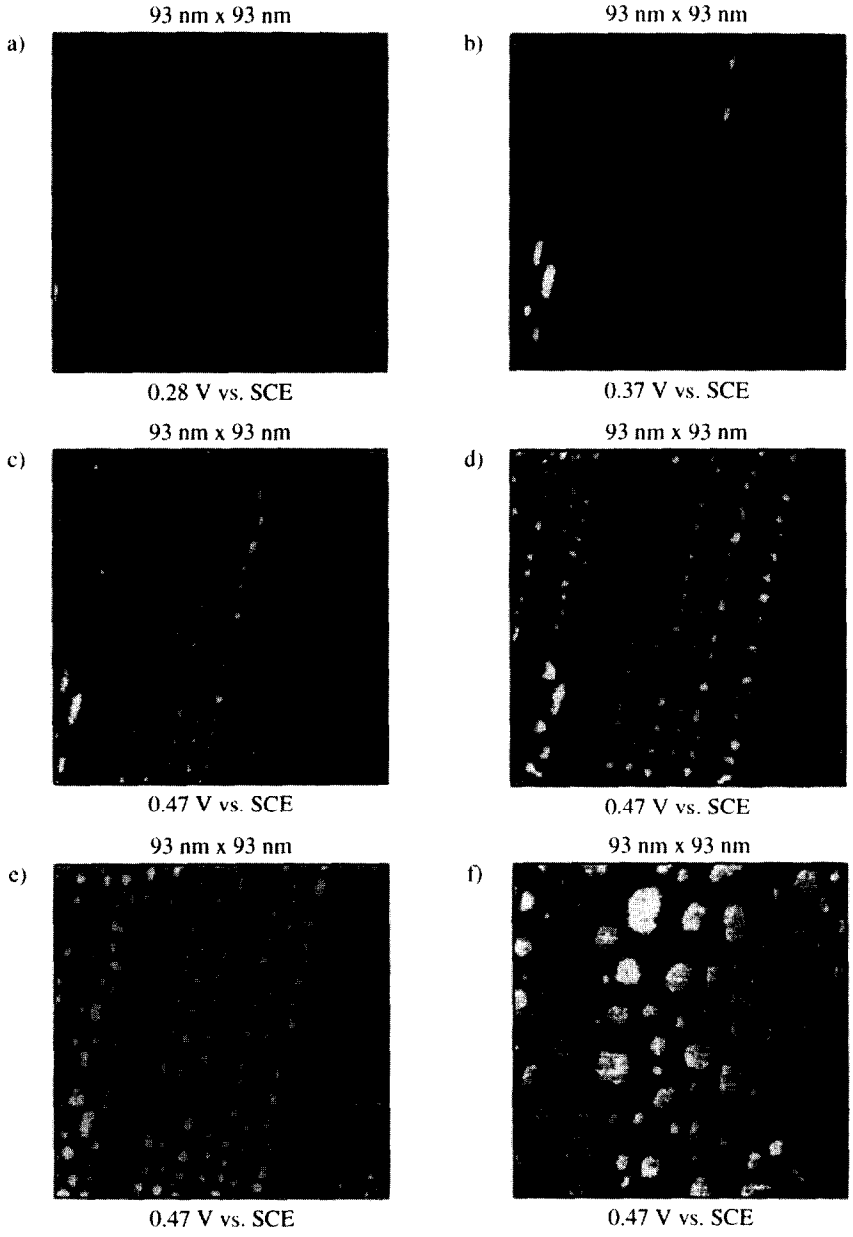

Fig. 8. Sequence of STM images, showing the structural changes of a reconstructed Au(100) surface in 0.1 M H_2SO_4 due to increasing positive electrode potentials. (a) $E = +0.28$ V vs. SCE; (b) $E = +0.37$ V vs. SCE; 05 min after (a); (c) $E = +0.47$ V vs. SCE; 06 min after (a); (d) $E = +0.47$ V vs. SCE; 07 min after (a); (e) $E = +0.47$ V vs. SCE; 09 min after (a); (f) $E = +0.47$ V vs. SCE; 24 min after (a).

move by slight shifts (see arrows) into the nearest 4-fold hollow sites (atoms 1 and 2 are already in 4-fold hollow sites). Hereby, the atoms are moving only by fractions of an atomic diameter. Due to this motion, atoms 7, 8 and 9 which are on top sites in the (hex)-structure are expelled onto the surface. This process is continued along one reconstruction row. Atoms 7, 8 and 9 and all other atoms of this row which are expelled onto the surface during the transition form the monoatomic-high gold islands

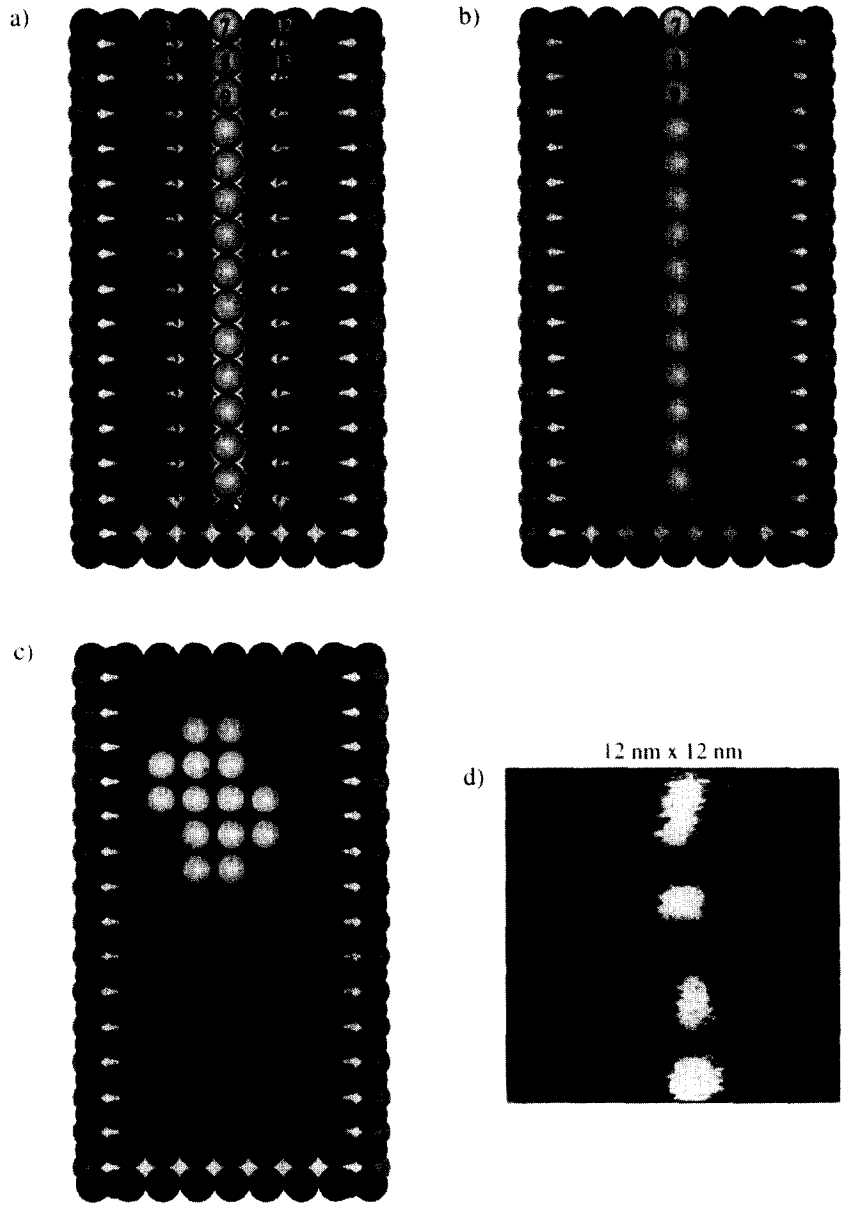

Fig. 9. (a–c) Model of the suggested mechanism for the initial stages of the (hex)→(1×1) structural transition (smaller balls represent the atoms of the topmost layer). (d) STM image of a reconstructed Au(100) surface in 0.01 M H_2SO_4, showing the initial stages of the (hex)→(1×1) transition: One single row has been lifted. $E = -0.34$ V vs. SCE.

created upon lifting of the reconstruction. The single atoms expelled onto the surface (Fig. 9(b)) condense immediately by surface diffusion into small, round shaped islands with a size being confined exactly at the position of expelled row of atoms (7, 8, 9) (Fig. 9(c)). (The arrangement of the topmost atoms in Fig. 9(b) is highly unstable.) In Fig. 9(a) (lower part of the image) it is demonstrated that the beginning of the structural transition is most favourable at defects such as missing rows: the shift of atoms (e.g. atom *a* and *b* where atoms *a*, *b* and *c* mark a defect) into 4-fold hollow sites is now possible with less dis-

placement of other atoms of the (hex)-phase (see arrows in Fig. 9(a)), because there is no other atom of the reconstructed phase sitting on atom *c*. An analogous effect exists if the atoms already expelled onto the surface condense to small islands. In this case defects are formed which are similar to those of the missing rows and therefore the continuation of lifting of reconstruction is also favoured. That means if a small (diameter at least 1 nm) unreconstructed island is once formed, the continuation of the (hex)→(1×1) transition is much easier.

To summarize, it was found that the (hex)→(1×1) transition is highly anisotropic and proceeds along the reconstruction rows, the 'unzipping' of the (hex)-structure starting at the top of the reconstruction row, where the surface atoms are in 'on top' positions. This is concluded from the location of the gold islands after lifting of one single reconstruction row (Fig. 9(d)).

5.2. Surface diffusion

Observation of the small monoatomic-high gold islands which are formed on Au(100)-(1×1) immediately after lifting of the reconstruction and their change with time have revealed an anion enhanced mobility of gold atoms [22,30]. This increased surface diffusion leads to a mobility of small islands on the unreconstructed surface which is demonstrated in a sequence of STM images in Fig. 10. The first image (a bottom to top scan) was started with a reconstructed Au(100) surface, then the potential was stepped to positive values (see arrow) and – as expected – the formation of gold islands starts. With time the number of islands decreases while their size increases. The decrease in the island density reflects the fact that in the later stages the island growth proceeds via a two-dimensional Ostwald ripening process. That means smaller islands are removed and larger islands grow at the expense of the smaller ones, due to statistical fluctuations at the rims of the islands. In Fig. 10(b–f) there are several examples showing this mechanism; one example for the disintegration of two small islands in the vicinity of bigger ones being marked by a circle. In this sequence it is also demonstrated that the mobility of gold atoms increases not only with time but also with potential, which of course is limited to the double-layer charging region. A consequence of this anion enhanced mobility is the rather quick disappearing of gold clusters and other surface irregularities at positive electrode potentials. This, obviously, leads to an improvement of the quality of single crystal surfaces and is therefore employed to restore in-situ and at room temperature the quality of surfaces after maltreatment of the electrodes by oxidation, corrosion, alloying or similar events. This smoothing effect has been termed electrochemical annealing [31–33].

After we have seen that the thermally induced reconstruction is stable in an electrochemical environment at sufficiently negative potentials and this reconstruction is lifted by changing the electrode potential in anodic direction, the question arises, what happens with an unreconstructed Au(100) surface when we apply again negative potentials to the electrode? This question will be answered in the next section.

6. Potential induced reconstruction

In the first image of Fig. 11 (a top to bottom scan) there was initially a perfectly reconstructed Au(100) surface obtained after flame annealing. The potential was then changed in three steps from −0.19 V vs. SCE in positive direction to +0.52 V vs. SCE, resulting in the reconstruction being completely lifted due to anion adsorption. In the following STM scan the electrode potential was again stepped to negative values and it can be seen that reconstruction rows were slowly formed along the two main crystallographic directions of the square substrate lattice. Fig. 11(c) and (d) represents the same surface area as in the first two scans, but after 14 min and 24 min, respectively, holding the potential at −0.22 V vs. SCE. This potential induced reconstruction follows a nucleation-and-growth behaviour where the rims of the many gold islands – which had been created during lifting of reconstruction – now act as nucleation centres. An example is shown in Fig. 11(b) where a reconstruction row (between the two arrows) starts at the rims of monoatomic-high gold islands. As a consequence, the (hex)-domains are now much smaller than those for thermally induced reconstruction and the directions of the reconstruc-

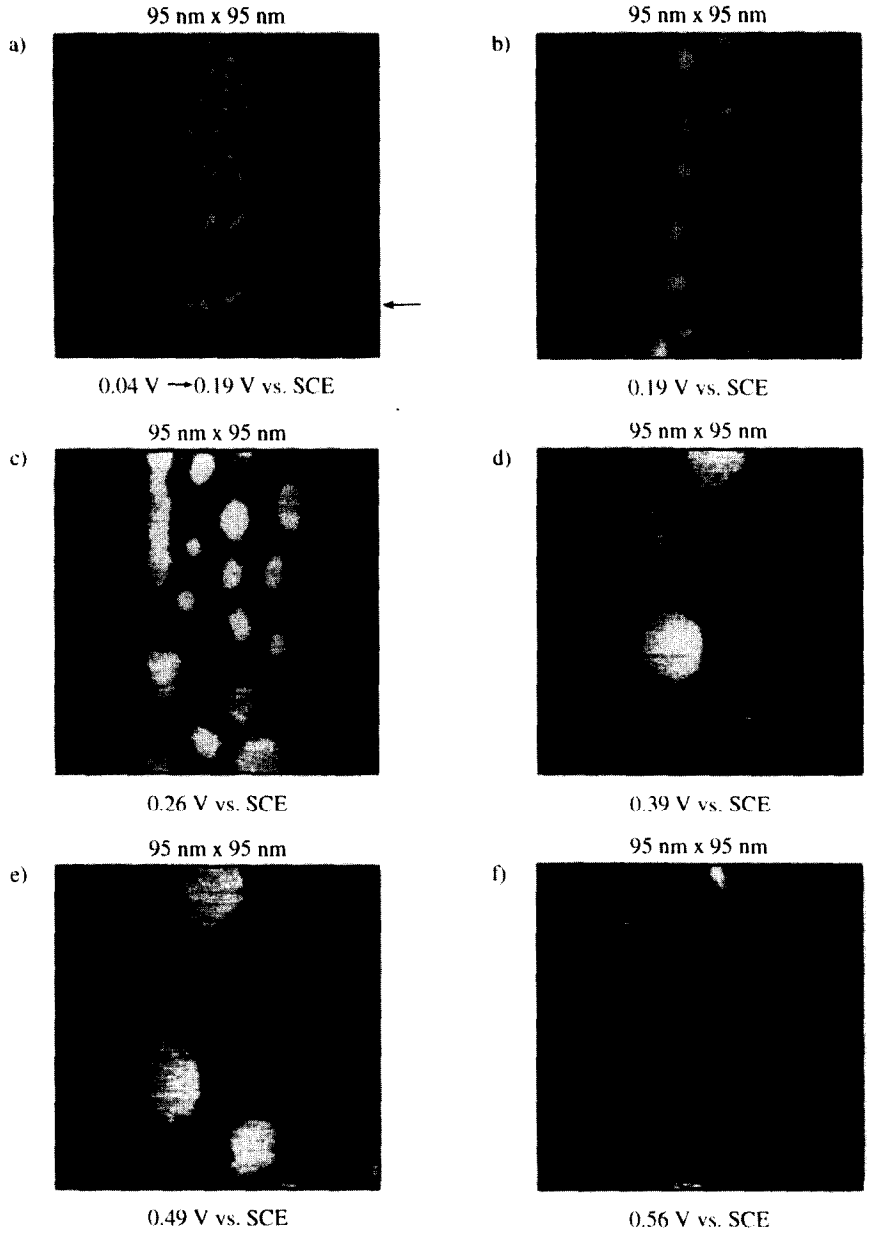

Fig. 10. Series of STM images of Au(100) in 0.1 M H_2SO_4, showing the coarsening of gold islands after the potential was stepped to positive values. (a) Stepping the potential from $E = +0.04$ V to $+0.19$ V vs. SCE; (b) $E = +0.19$ V vs. SCE; 08 min 00 s after (a); (c) $E = +0.26$ V vs. SCE; 09 min 20 s after (a) and 0 min 00 s at this potential; (d) $E = +0.39$ V vs. SCE; 22 min 40 s after (a) and 1 min 20 s at this potential; (e) $E = +0.49$ V vs. SCE; 25 min 20 s after (a) and 1 min 20 s at this potential; (f) $E = +0.56$ V vs. SCE; 33 min 20 s after (a) and 1 min 20 s at this potential.

tion rows are about equally distributed among the two main crystallographic directions of the substrate. The driving force for this $(1\times1)\rightarrow$(hex) structural transition is a negative surface excess charge which is induced by the negative electrode potential. Such surface excess charges can obviously lower the

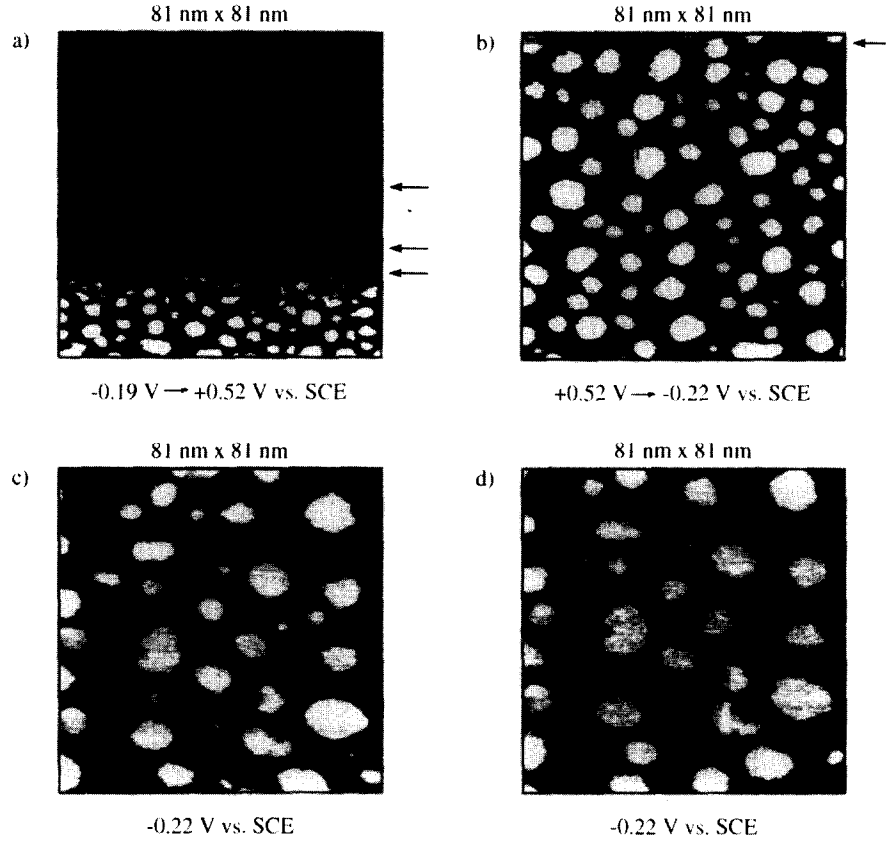

Fig. 11. Sequence of STM images for an Au(100) electrode in 0.1 M H_2SO_4, showing a potential induced reconstruction. In image (a), the potential for a freshly prepared Au(100)-(hex) surface was stepped in three steps from $E = -0.19$ V to $+0.52$ V vs. SCE, where reconstruction was lifted. In the following image (b), the potential was stepped back to $E = -0.22$ V vs. SCE and the slow formation of the (hex)-structure appears which is seen by the increasing number of reconstruction rows. (c and d) $E = -0.22$ V vs. SCE, 14 min and 24 min, respectively, at that potential.

activation barrier for reconstruction to the extent that this potential or charge induced reconstruction becomes possible even at room temperature.

STM studies [22,29,34] have also revealed that the gold islands of the unreconstructed surface do not only provide with their rims the starting points for the $(1\times1)\rightarrow$(hex) transition, they also supply by disintegration the additional Au atoms required for the formation of the more densely packed (hex)-rows and -domains. This is demonstrated for example in Fig. 11(c), where a small gold island (within the white circle) delivers material to form a new reconstruction row (marked by an arrow in Fig. 11(d)).

One point is worth emphasizing: Once the monoatomic-high gold islands have disappeared due to extensive Ostwald ripening or electrochemical annealing (see Section 5) and with them the vast majority of nucleation centres for the $(1\times1)\rightarrow$(hex) transition, it seems to be almost impossible to have any significant potential induced reconstruction, say within about 1 h. This demonstrates the importance of nucleation centres for the structural transitions to occur within a reasonable amount of time.

From a comparison of a thermally induced reconstructed (e.g. Fig. 4 or Fig. 6(a) and (b)) and a potential induced reconstructed (e.g. Fig. 12) Au(100) surface it becomes obvious that the structures and hence the properties of both surfaces are sufficiently different to justify this distinction: A potential induced reconstructed surface – which exists only for the metal/electrolyte interface – may still partly be unreconstructed with small recon-

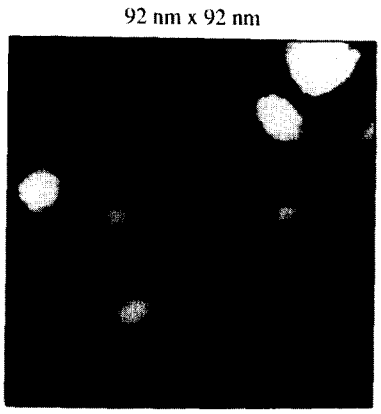

Fig. 12. STM image of Au(100) in 0.1 M H_2SO_4, showing potential induced reconstruction. $E = -0.19$ V vs. SCE.

structed domains and show different orientations on one and the same terrace, whereas the thermally induced reconstruction often shows only one single (hex)-domain per terrace. Because of the much higher number of imperfections at a reconstructed surface which was obtained at negative potentials, the kinetics of structural transitions on such a surface can differ significantly from that on a thermally prepared one.

The potential induced reconstruction which is shown here for Au(100) and which has also been found for the other two low index faces of gold could have far-reaching consequences for structure-sensitive reactions such as adsorption reactions. Therefore, when studying such types of reactions, the potential dependent structure of an Au(100) surface should always be taken into account. One example is the adsorption of pyridine on an Au(100) electrode. It has been observed that, at potentials negative with respect to the pzc, pyridine is adsorbed flat on Au(100), whereas at potentials positive with respect to the pzc the molecule is in an upright position. However, only with the detailed knowledge about potential induced surface reconstruction it became clear that the flat-lying pyridine is adsorbed on the reconstructed, (111)-like gold surface. The structural transition from flat to vertical was found to occur simultaneously with lifting of the reconstruction. On the unreconstructed Au(100), on the other hand, pyridine was shown to adsorb in a vertical position from the very beginning [35].

7. Summary

The surface structure of well prepared gold single crystal electrodes may often be quite different from that expected by simple bulk crystallographic considerations. An important structural feature of low index Au(*hkl*) are surface reconstructions. In this study it has been demonstrated that flame annealed Au(100) electrodes have reconstructed surfaces which have different electrochemical properties than their unreconstructed counterparts. (Details about reconstruction phenomena also for Au(110) and Au(111) mainly derived from STM studies are summarized in a recent review article [36]). However, well prepared reconstructed Au(100) surfaces require slow cooling after flame annealing. The frequently advocated fast quenching in water results in structurally ill-defined, defect-rich surfaces.

Lifting of the reconstruction leads to the formation of monoatomic-high gold islands on the surface, which inevitably adds to the surface imperfections. Holding the electrode potential at potentials sufficiently positive with respect to the pzc results in large, atomically flat unreconstructed terraces due to an electrochemical annealing.

Once the initial (thermally induced) reconstruction of a Au(100) surface had disappeared, e.g. due to specific adsorption of anions, a potential induced reconstruction may take place, usually at potentials clearly negative with respect to the pzc. As a consequence, the surface structure of a gold electrode is potential dependent and structural changes may occur within the potential region chosen for an experiment.

References

[1] R. Parsons and T. VanderNoot, J. Electroanal. Chem. 257 (1988) 9.
[2] R.R. Adžić, N.M. Marković and V.B. Vešović, J. Electroanal. Chem. 165 (1984) 105, 121.
[3] K. Jüttner and W.J. Lorenz, Z. Phys. Chem. NF 122 (1980) 163.
[4] G.A. Somorjai and M.A. Van Hove, Progr. Surf. Sci. 30 (1989) 201.
[5] K. Takayanagi, Ultramicroscopy 8 (1982) 145.
[6] G. Binnig, H. Rohrer, C. Gerber and E. Weibel, Surf. Sci. 131 (1983) L379.

[7] D.G. Fedak and N.A Giostein, Surf. Sci. 8 (1967) 77.
[8] M.A. Van Hove, R.J. Koestner, P.C. Stair, J.P. Bibérian, L.L. Kesmodel, I. Bartoš and G.A. Somorjai, Surf. Sci. 103 (1981) 189, 218.
[9] W. Moritz and D. Wolf, Surf. Sci. 163 (1985) L655.
[10] J. Möller, H. Niehus and W. Heiland, Surf. Sci. 166 (1986) L111.
[11] R.M. Penner, M.J. Heben and N.S. Lewis, Anal. Chem. 61 (1989) 1630.
[12] L.A. Nagahara, T. Thundat and S.M. Lindsay, Rev. Sci. Instrum. 60 (1989) 3128.
[13] C.E. Bach, R.J. Nichols, W. Beckmann, H. Meyer, A. Schulte, J.O. Besenhard and P.D. Jannakoudakis, J. Electrochem. Soc. 140 (1993) 1281.
[14] D.M. Kolb, R.J. Nichols and R.J. Behm, in: Electrified Interfaces in Physics, Chemistry and Biology, ed. R. Guidelli (NATO ASI Vol. C 355, Kluwer, Dordrecht, 1992) p. 275
[15] K. Heinz, E. Lang, K. Strauss and K. Müller, Appl. Surf. Sci. 11/12 (1982) 611.
[16] G. Ertl, Surf. Sci. 152/153 (1985) 328.
[17] A. Hamelin, J. Electroanal. Chem. 142 (1982) 299.
[18] E. Yeager, A. Homa, B.D. Cahan and D. Scherson, J. Vac. Sci. Technol. 20 (1982) 628.
[19] A.S. Homa, E. Yeager and B.D. Cahan, J. Electroanal. Chem. 150 (1983) 181.
[20] D.M. Kolb and J. Schneider, Electrochim. Acta 31 (1986) 929.
[21] D.M. Kolb, in: Structure of Electrified Interfaces, eds. J. Lipkowski and P.N. Ross (VCH, New York, 1993) pp. 65–102.
[22] O.M. Magnussen, J. Hotlos, R.J. Behm, N. Batina and D.M. Kolb, Surf. Sci. 296 (1993) 310.
[23] J. Clavilier, R. Fauré, G. Guinet and R. Durand, J. Electroanal. Chem. 107 (1983) 181.
[24] A. Hamelin and A. Katayama, J. Electroanal. Chem. 117 (1981) 221.
[25] N. Batina, A.S. Dakkouri and D.M. Kolb, J. Electroanal. Chem. 370 (1994) 87.
[26] U.W. Hamm and D.M. Kolb, J. Electroanal. Chem. 332 (1992) 339.
[27] P. Skoluda, U.W. Hamm and D.M. Kolb, J. Electroanal. Chem. 354 (1993) 289.
[28] P. Skoluda and D.M. Kolb, Surf. Sci. 260 (1992) 229.
[29] A.S. Dakkouri, Ph.D. Thesis, University of Ulm (1996).
[30] D.M. Kolb, A.S. Dakkouri and N. Batina, in: Nanoscale Probes of the Solid/Liquid Interface, eds. A.A. Gewirth and H. Siegenthaler (NATO ASI Vol. E 288, Kluwer, Dordrecht, 1995) p. 263.
[31] J.L. Stickney, I. Villegas and C.B. Ehlers, J. Am. Chem. Soc. 111 (1989) 6473.
[32] G.J. Cali, G.M. Berry, M.E. Bothwell and M.P. Soriaga, J. Electroanal. Chem. 297 (1991) 523.
[33] T. Will, M. Dietterle and D.M. Kolb, in: Nanoscale Probes of the Solid/Liquid Interface, eds. A.A. Gewirth and H. Siegenthaler (NATO ASI Vol. E 288, Kluwer, Dordrecht, 1995) p. 137.
[34] X. Gao, G.J. Edens, A. Hamelin and M.J. Weaver, Surf. Sci. 296 (1993) 333.
[35] P. Skoluda, M. Hölzle, J. Lipkowski and D.M. Kolb, J. Electroanal. Chem. 358 (1993) 343.
[36] D.M. Kolb, Progr. Surf. Sci. 51 (1996) 109.